Materials Science-Poland, 37(2), 2019, pp. 196-205
http://www.materialsscience.pwr.wroc.pl/
DOI: 10.2478/msp-2019-0021

sciendo

Structural, optical, thermal, dielectric and mechanical studies of a new organic NLO material: L-isoleucinium p-toluenesulfonate monohydrate (LIPT)

M. SURESH[1,*], S. ASATH BAHADUR[2], S. ATHIMOOLAM[3]

[1]Department of Physics,Er. Perumal Manimekalai College of Engineering, Hosur, Tamil Nadu-635117, India
[2]Department of Physics, Kalasalingam Academy of Research and Education, Krishnankoil, Tamil Nadu - 626 190, India
[3]Department of Physics, University College of Engineering, Anna University Constituent College, Nagercoil, Tamil Nadu - 629 004, India

In the present work, a new organic second order NLO material: L-isoleucinium p-toluenesulfonate monohydrate (LIPT) is synthesized and reported for the first time. The LIPT is crystallized in a non-centrosymmetric monoclinic space group $P2_1$. Structural and hydrogen bond nature of the compound is analyzed using single crystal X-ray diffraction studies. The crystal exhibits very good optical properties such as wide optical transparency in the region of 210 nm to 1100 nm and the ultraviolet wavelength emission ($\lambda = 283$ nm). The second harmonic generation efficiency is found to be 1.7 times the standard KDP. Good thermal, mechanical properties and low dielectric constant at high frequency range show that the material may be a potential candidate for optoelectronic applications.

Keywords: *optical material; SHG; single crystal XRD; TGA/DTA; UV spectrum*

1. Introduction

The search for new NLO materials with enhanced NLO properties have been showing a great deal of interest due to their potential applications in the photonic technologies. Among the NLO materials, organic materials find extra attention due to their interesting features. Conjugated π bond and lack of inversion symmetry are the most expected features of NLO crystals for their potential applications [1, 2].

To reach the above mentioned expectations and to attain the acentric crystal structure, various molecular engineering approaches have been recommended. In the diverse strategies available, hydrogen bonding interactions play a key role in reaching the desired crystal structure of organic molecules by orienting the molecular dipoles in a head to tail manner [3, 4]. It also improves the mechanical and thermal stabilities. Hydrogen bonding supplemented by a mutual polarization will also give rise to an efficient second harmonic generation.

Among the broad category of organic NLO crystals, amino acids exhibit specific features such as chiral crystallographic structure, wide transparency window in the visible region and zwitterionic nature, and they can be used as a basis for synthesizing organic compounds and derivatives with an acentric crystal structure which is very important for enhanced NLO activity. Under the above facts, the amino acids are found to be well established root to attain the expected structural features which may improve NLO activities of the material. Thus, a large number of amino acids and their derivatives have been studied for NLO applications. L-histidinium p-toluenesulfonate (LHPT) [5], L-alaninium p-toluenesulfonate (LAPT) [6], L-valinium p-toluenesulfonate monohydrate (LVPT) [7] and L-leucinium p-toluenesulfonate monohydrate (LLPT) [8] are some of the amino acid based NLO materials reported earlier by our laboratory.

*E-mail: sureshmuthu23@yahoo.com

In this series, efforts were taken to synthesize a new NLO material using L-isoleucine, an amino acid and p-toluenesulfonic acid monohydrate. The p-toluenesulfonic acid monohydrate is a strong acid forming strong hydrogen bonding complexes with bases like amines. A large number of charge transfer complexes of p-toluenesulfonicacid with acentric crystal structure have been reported recently [9–13]. L-isoleucine is the branched-chain α-amino acid with the chemical formula $C_6H_{13}NO_2$. Isoleucine is classified as a hydrophobic amino acid due to its hydrocarbon side chain. The NLO activity of L-isoleucinium picrate [14] and L-isoleucinium bromide [15] being a kind of L-isoleucine compound have been reported recently.

In the present work, a new amino acid, p-toluenesulfonate monohydrate compound, namely L-isoleucinium p-toluenesulfonate monohydrate (LIPT) has been synthesized. Its structural features and important material properties are reported here.

2. Experimental

2.1. Material synthesis and crystal growth

Commercially available p-toluenesulfonic acid monohydrate and L-isoleucine were used to synthesize the title compound according to reaction scheme shown in the Fig. 1. The solution was prepared using water as a solvent with the precursor materials taken in the 1:1 equimolar ratio. The synthesized salt was purified by a successive recrystallization process with water as a solvent.

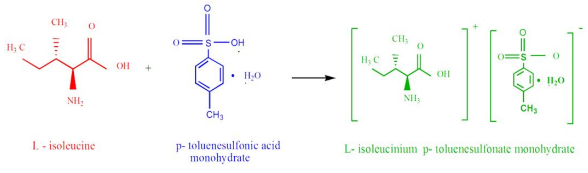

Fig. 1. Reaction scheme for L-isoleucinium p-toluenesulfonate monohydrate (LIPT).

The single crystal growth of the title compound was performed using a solution prepared from the synthesized salt with water as a solvent. The prepared growth solution was kept in a constant temperature bath with an accuracy of ±0.01°C. After a span of 10 days, tiny single crystals of characteristic shape and size were harvested. A small crystal of characteristic shape and size with good transparency was used as a seed for bulk growth. Bulk crystal growth was undertaken by submerged-seed solution growth method by immersing the seed inside the prepared supersaturated solution. The bulk crystals of the size 24 mm × 23 mm × 10 mm were obtained in a period of 20 days. The grown crystal of synthesized compound is shown in Fig. 2.

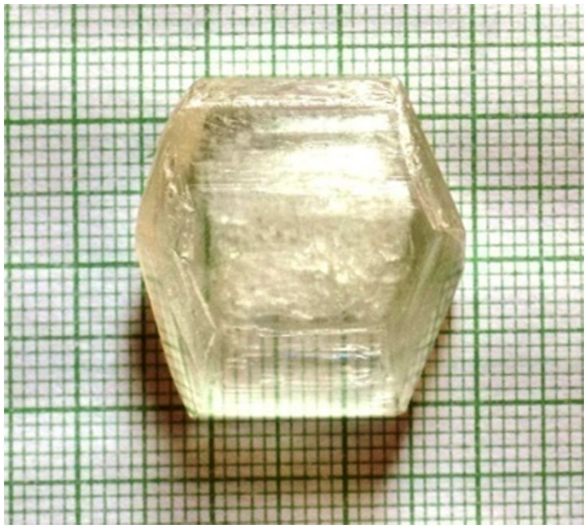

Fig. 2. The grown LIPT single crystal (24 mm × 23 mm × 10 mm).

2.2. Characterization

Unit cell parameters of a single crystal of the title compound were calculated from single crystal X-ray diffraction studies carried out by using ENRAF NONIUS CAD4-MV31single crystal X-ray diffractometer (graphite-monochromated, MoKα = 0.71073 Å). After confirming the new phase of the material by the Cambridge Structural Database (CSD), the complete data collection of the crystal was recorded with the same instrument. The unit cell parameters of the crystal were obtained from least-square refinement of centered reflections (Table 1). The structure was solved and refined with the SHELXL-14 program [16]. All the atoms except H atoms were refined anisotropically. All the H atoms except hydrogen atoms participating in classical hydrogen bonds were positioned

geometrically and refined using the riding model with C–H = 0.3 to 0.96 Å, and U_{iso} (H) = 1.2 to 1.5U_{eq}(C). The H atoms which were involved in hydrogen bonds were located from electron density map and refined isotropically. The convergence of the structure was confirmed by the R-factor [3.05 % for $I > 2\sigma(I)$]. The observed absolute structure parameters (Flack parameter) of the compounds confirm the chiral nature of the compound.

The crystallographic data, details of data collection and the structure refinement are given in Table 1. The selected bond lengths, angles and torsional geometries of LIPT are given in Table 2. The hydrogen bonding dimensions are listed in Table 3. Fig. 3 shows an ORTEP view of the molecules drawn at 50 % probability thermal displacement ellipsoids with the atom numbering scheme. The hydrogen bonding networks and the packing arrangement of molecules are depicted in Fig. 4 with the necessary graph-set notations. Linear optical properties of the material were analyzed by UV-Vis-NIR absorption spectrum in the wavelength range of 200 nm to 1100 nm using the UV-1700 Shimadzu spectrometer with the resolution of 1 nm. The emission spectrum of the compound was recorded using Cary Eclipse spectrophotometer. The thermal behavior of the material was studied by simultaneous TG/DTA analyses in the temperature range of 20 °C to 500 °C using SEIKO TG/DTA 6200 analyzer, in a nitrogen atmosphere at the heating rate of 20 °C/min. The dielectric nature of the material was studied by employing a HIOKI multi frequency LCR meter. The Vicker's microhardness tester was used to assess the mechanical properties of the grown crystal at varying loads from 25 g to 100 g. The SHG efficiency was measured by employing Kurtz and Perry powder technique using a Q-switched mode locked Nd:YAG laser of a wavelength 1064 nm.

3. Results and discussion

3.1. Molecular structure determination and crystal packing

From the single crystal X-ray diffraction studies, it was found that the compound crystallized

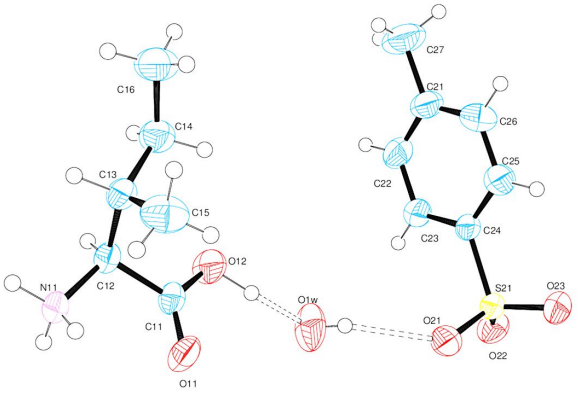

Fig. 3. ORTEP diagram of the compound (LIPT) with 50 % thermal displacement ellipsoid and atom numbering scheme.

in the monoclinic system with cell parameters a = 10.190(5) Å, b = 6.571(3) Å, c = 12.758(6) Å, β = 104.3(1) and space group $P2_1$. The asymmetric part of the crystal consists of L-isoleucinium cation, p-toluenesulfonate anion and a lattice water molecule. The C–O bond lengths (1.200 (2) and 1.301 (2) Å) of the carboxyl group in the cation clearly indicate the existence of –COOH group. The protonation of the amino N atom is confirmed by the lengthened C–N bond distance (1.486 (2) Å) and the intermolecular interactions leading to deviation of the N atom from the plane of the carboxyl group of about 0.343 (2) Å. The plane of the carboxyl group of the cation and the plane of the aromatic ring of the anion are inclined at an angle of 54.3 (2)°. The backbone conformations ψ^1 and ψ^2 of the L-isoleucinium cation are observed to be trans and cis forms, respectively. Similarly, the side chain conformations, *viz.*, χ^1 and χ^2 are observed as –165.1 (1)° and 165.6 (2)°, respectively.

The single crystal XRD studies show that all the three hydrogen atoms of amino group in the cation are hydrogen bonded to the O atoms of the p-toluenesulfonate anion. The crystal structure is stabilized through three-dimensional hydrogen bonding network formed by three N–H…O and three O–H…O hydrogen bonds (Table 3). The water molecule makes exclusive hydrogen bonding interactions with the cation and anion. One of the H atoms from the amino group is connected with

Table 1. Crystallographic data for LIPT single crystal.

Compound	L-isoleucinium p-toluenesulfonate monohydrate (LIPT)
Empirical formula	$(C_6H_{14}NO_2S)^+ \cdot (C_7H_7SO_3)^- \cdot H_2O$
Formula weight	321.38 g/mol
Temperature	293(2) K
Wavelength	0.71073 Å
Crystal system, Space group	Monoclinic, $P2_1$
Unit cell dimensions	a = 10.190(5) Å; $\alpha = 90°$
	b = 6.571(3) Å; $\beta = 104.344(1)°$
	c = 12.758(6) Å; $\gamma = 90°$
Volume, Z	827.62(7) $Å^3$, 2
Density (calculated)	1.290 mg/m^3
Absorption coefficient	0.220 mm^{-1}
F(000)	344
Crystal size used for XRD	0.23 mm × 0.22 mm × 0.21 mm
Theta range for data collection	1.65° to 30.20°
Index ranges	$-14 \leqslant h \leqslant 14, -9 \leqslant k \leqslant 9, -17 \leqslant l \leqslant 17$
Reflections collected	20934
Independent reflections	4523 [R(int) = 0.0248]
Refinement method	Full-matrix least-squares on F^2
Data/restraints/parameters	4523/1/217
Goodness-of-fit on F2	1.096
Final R indices [I>2sigma(I)]	R1 = 0.0305, wR2 = 0.0760
R indices (all data)	R1 = 0.0386, wR2 = 0.0867
Absolute structure parameter	–0.05(5)
Largest diff. peak and hole	0.222 and –0.284 e. $Å^{-3}$
CCDC No.	1478186

the O atoms of the anion leading to bifurcated ring $R_1^2(4)$ motif. Further, this bifurcated N–H...O hydrogen bond interacts with water molecule through the O–H...O hydrogen bond forming a ring $R_3^3(9)$ motif. These two ring motifs, connected with the two O–H...O hydrogen bonds, lead to two parallel chain $C_3^3(11)$ motifs extending along the c-axis of the unit cell. These chains are cross-linked through a N–H...O hydrogen bond leading to two alternate ring motifs, viz., ring $R_5^5(17)$ and $R_4^4(10)$ motifs, along the same axis. These ring and chain motifs lead to the hydrophobic layers at x = 0 and 1 which are sandwiched between the hydrophilic layers at x = 1/2 (Fig. 4).

Symmetry transformations used to generate equivalent atoms: #1 –x+2, y+1/2, –z+2; #2 –x+2, y+1/2, –z+1; #3 x+1, y+1, z; #4 x+1, y, z; #5 x–1, y, z.

3.2. Thermal analysis

Thermal behavior of the title compound is depicted in Fig. 5. The absence of a significant change in the TGA curve up to 110 °C indicates that the compound remains in its monohydrous form. The weight loss (∼5 %) in the TGA curves at 110 °C indicates removal of water molecules from the compound as a result of which it becomes anhydrous. Further, the endothermic peak observed at 145 °C in DTA is assigned to the melting point of the compound. After the melting point, the compound experiences another weight loss around 15 % at a temperature of 225 °C. It may be assigned

Table 2. Selected geometric parameters of LIPT.

Atoms connected	Bond distance [Å]
C11–O11	1.200 (2)
C11–O12	1.301 (2)
C12–N11	1.486 (2)
O21–S21	1.445 (1)
O23–S21	1.455 (1)
O22–S21	1.455 (1)
Atoms connected	**Bond angle [°]**
O11–C11–C12	121.8 (1)
O12–C11–C12	112.6 (1)
O21–S21–O23	112.4 (8)
O21–S21–O22	112.6 (8)
O23–S21–O22	110.3 (7)
Atoms connected	**Torsion angle [°]**
N11–C12–C11–O11	–17.2 (2)
N11–C12–C11–O12	164.4 (1)
N11–C12–C13–C14	–165.1 (1)
C12–C13–C14–C16	165.6 (2)

Table 3. Hydrogen bonding geometry in LIPT

D–H···A [Å, °]	d(D–H) [Å]	d(H···A) [Å]	d(D···A) [Å]	<(D–H···A) [°]
O1W–H2W…O21	0.75 (4)	2.13 (3)	2.826 (2)	156
O12–H12...O1W$^{\#1}$	1.03(3)	1.53 (3)	2.551 (2)	172
N11–H11A...O22$^{\#2}$	0.93 (2)	2.01 (2)	2.899 (2)	158
N11–H11B...O23$^{\#3}$	0.90 (2)	1.92 (2)	2.804 (2)	165
N11–H11C...O22$^{\#4}$	0.90 (2)	2.00 (2)	2.820 (2)	151
O1W–H1W...O11$^{\#5}$	0.81 (6)	2.00 (5)	2.768 (2)	157

to the liberation of NH_3 group. An endothermic peak observed at 280 °C in DTA curve is assigned to the decomposition temperature of the compound. Further, in the temperature range between 225 °C to 375 °C, the compound suffers major weight loss as indicated in TGA. It might have happened due to the loss of CH_4 and gaseous products such as SO_3, CO and hydrocarbon gases, one by one.

3.3. Vicker microhardness test

A well-polished crystal with smooth surface was used and static indentations were made at room temperature with a constant indentation time of 10 second on the smooth (0 0 1) face of the crystal with the load varying from 25 g to 100 g using Vicker's microhardness tester. The hardness number was calculated using the relation:

$$H_v = \frac{1.8544\ P}{d^2} \tag{1}$$

where P is the applied load in kg and d is the diagonal length of the indentation impression in micrometer. The variation of calculated hardness number H_v versus load P applied to the crystal is depicted in Fig. 6a. The figure suggests

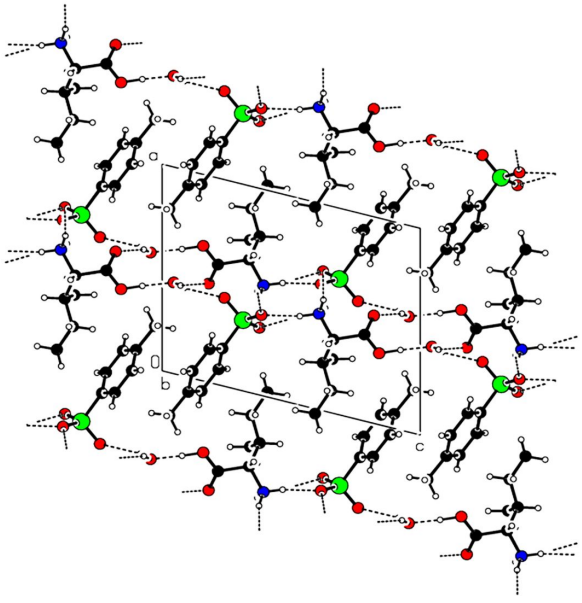

Fig. 4. Packing diagram of LIPT viewed down the b-axis of the unit cell showing alternate hydrophobic (at 0 and 1) and hydrophilic layers (at 1/2) along *a*-axis. The intermolecular hydrogen bonds are shown as dashed lines.

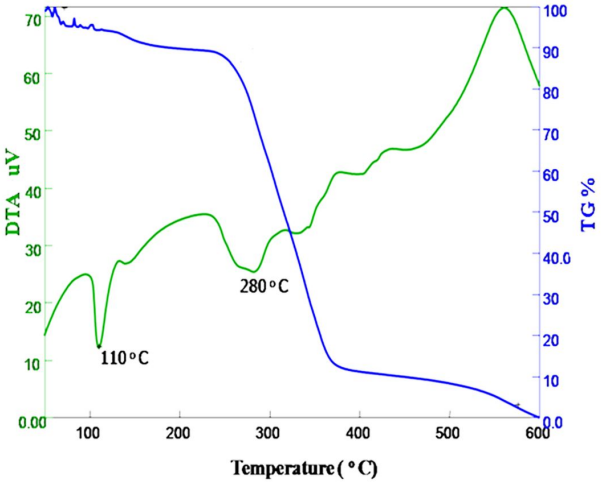

Fig. 5. DTA/TGA curve of LIPT.

that the microhardness number is increasing with the increase in load, as is observed in most organic compounds, and shows the reverse indentation size effect (RISE) in the studied crystal. This is also the indication of dominant plastic deformation on the surface of the studied crystal [17, 18].

For the indentation load above 100 g, cracks are initiated on the crystal surface, around the indenter. This is due to the release of internal stress locally initiated by indentation. The observed relatively higher hardness values of LIPT compared to some of organic NLO crystals [19] indicate that the average bond strength and the number of bonds per unit volume in the solid structure may be the reason for the results.

The Meyer index n calculated from the slope of straight line obtained in the plotted graph between log P and log d (Fig. 6b) gives the hardness category of crystal. The slope value identified from the straight line fitted from the figure is n = 2.16. Since n>2, crystals could be classified as soft material [20]. Hence, extra care needs to be taken while using these materials for device fabrication.

3.4. Dielectric studies

The crystal was polished and its opposite faces were coated with air-drying silver paste to construct it as a parallel plate capacitor. Dielectric properties of the compound were analyzed using the measured capacitance C and dissipation factor D values of the sample at different frequencies at room temperature. Dielectric constant ϵ_r and dielectric loss tanδ values were calculated using the relation:

$$\varepsilon_r = C/C_o \tag{2}$$

and

$$\tan\delta = \varepsilon_r D \tag{3}$$

The response of the grown single crystals to applied electric field as a function of dielectric constant with varying frequency were recorded and plotted as shown in Fig. 7a. The dielectric constant values were found higher at lower frequencies than at higher frequencies. The high values of dielectric constant at low frequency may be due to the presence of all polarizations and its low value at high frequency may be due to significant gradual loss of all polarizations [21]. The calculated dielectric constant ϵ_r of the compound was found as 35.8 and it is relatively larger than that of electro optic crystal DAST ($\epsilon_r = 5.2$) [22, 23] and noticeably lower

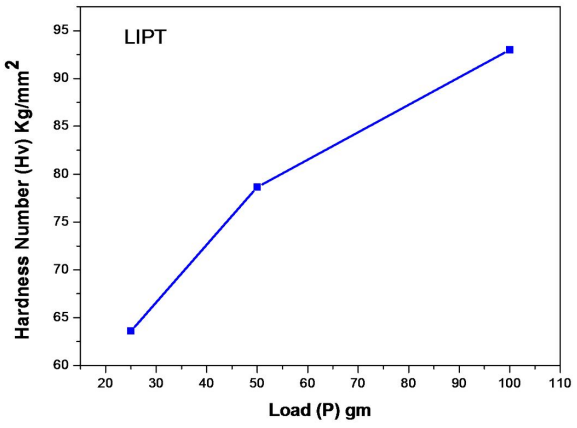

(a)

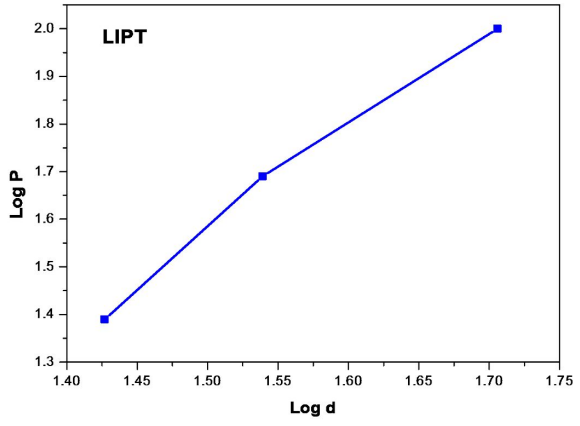

(b)

Fig. 6. (a) hardness number H_V vs. load (P) for LIPT; (b) log P vs. log d for LIPT.

than some those of inorganic electro optic crystals $LiNbO_3$ ($\epsilon_r = 85$), $KNbO_3$ ($\epsilon_r = 154$) [24].

The variation of dielectric loss as a function of frequency at room temperature is given in Fig. 7b. The graph shows the same trend as that observed for dielectric constant. The characteristic low values of dielectric loss at high frequencies for the LIPT crystal suggest that the crystal possesses enhanced optical quality with lesser defects and this parameter plays an important role in the fabrication of nonlinear optical devices [25]. Hence, it is concluded from the studies that the crystal of LIPT exhibits normal dielectric behavior. However, the variation observed in the plot of dielectric loss with respect to frequency suggests the possibility of presence of crystalline defects. In addition, the solid state parameters were calculated using the obtained value of dielectric constant and listed in Table 4. These values are compared with those of standard material KDP [26].

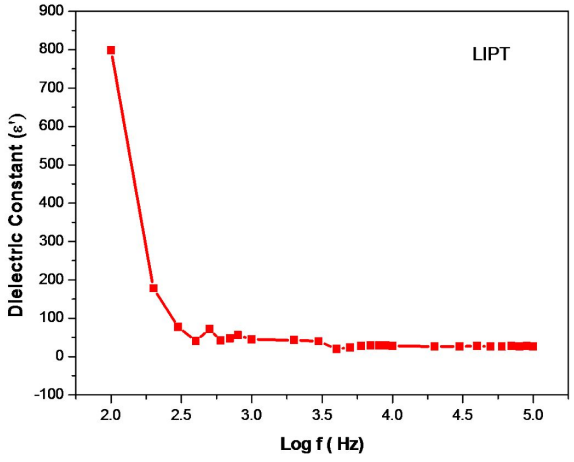

(a)

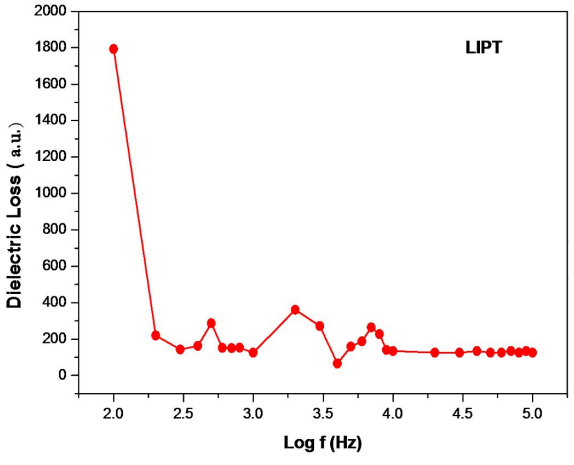

(b)

Fig. 7. (a) ϵ_r vs. log f for LIPT; (b) dielectric loss vs. log f for LIPT.

The solid state parameters were calculated to understand the dielectric nature of the material to analyze the NLO efficiency of the compound. The valence electron plasma energy ($\hbar\omega_p$) is given by:

$$\hbar\omega_p = 28.8\left(\frac{Z\rho}{M}\right)^{1/2} \tag{4}$$

here, the molecular weight M of LIPT = 321.3 g and the total number of valance electrons Z = 122.

The density ρ of the grown crystal = 1.290 g/cm^3 and dielectric constant ϵ_∞ = 35.8 (at 1 MHz frequency).

The Penn gap and Fermi energy is given by [27]:

$$E_P = \frac{\hbar\omega_p}{(\varepsilon_\infty - 1)^{1/2}} \tag{5}$$

Polarizability, α_e is obtained using the relation given by:

$$\alpha_e = \left[\frac{(\hbar\omega_p)^2 S_0}{(\hbar\omega_p)^2 S_0 + 3E_P^2}\right] \times \frac{M}{\rho} \times 0.396 \times 10^{-24} \tag{6}$$

where S_0 is a constant of the material, and is given by:

$$S_0 = 1 - \left[\frac{E_P}{4E_F}\right] + \frac{1}{3}\left[\frac{E_P}{4E_F}\right]^2 \tag{7}$$

The value of α_e obtained is in good agreement with the value calculated by Clausis-Mossetti equation, which is given by:

$$\alpha_e = \frac{3M}{4\pi\rho N_A}\left[\frac{\varepsilon_\infty - 1}{\varepsilon_\infty + 2}\right] \tag{8}$$

where $N_A = 6.023 \times 10^{23}$ is Avogadro number.

From the study, it is observed that the obtained values are found to be higher than those of KDP. As the NLO efficiency depends upon polarizability, it is evident that the NLO efficiency of the compound is expected to be comparatively greater than that of KDP.

3.5. Linear optical studies

3.5.1. UV-Vis-NIR spectral absorption studies

UV-Vis-NIR spectrum provides useful information about the electronic transition of the p-conjugated molecular systems. Fig. 8 shows the recorded UV-Vis-NIR absorption spectrum of the crystal sample of 1 mm thickness. The spectrum indicates the maximum absorption at 229 nm which is attributed to direct transition of an electron from a non-bonding n orbital to an antibonding π^* orbital ($n \rightarrow \pi^*$). In addition, one more shoulder peak is observed at 256 nm and it indicates the effect of transition of electrons from an antibonding π orbital to an antibonding π^* orbital ($\pi \rightarrow \pi^*$). The lower cut-off wavelength of the sample was recorded at 283 nm. This lower cutoff wavelength is important for NLO crystal efficient in the application in entire visible and near infrared region [28].

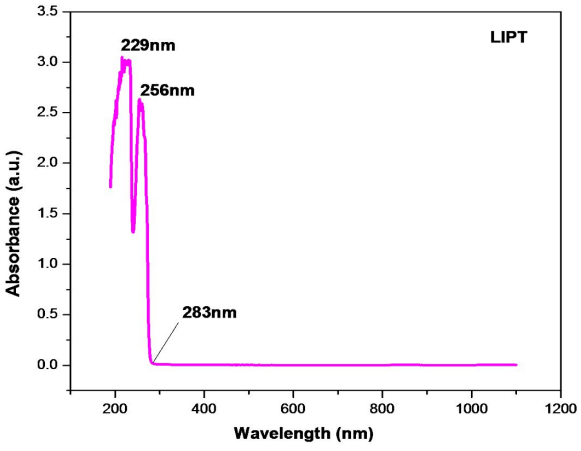

Fig. 8. UV-Vis-NIR absorbance spectrum of LIPT.

3.5.2. Photoluminescence studies

The photoluminescence spectrum of the compound was recorded using the crystal sample of 1 mm thickness in the wavelength range of 280 nm to 500 nm with an excitation wavelength of 280 nm (Fig. 9). The sharp intense peak observed around 291 nm may be due to the intra band transition ($n \rightarrow \pi^*$) between amino and C–O group of the compound. The peak around 291 nm also indicates the ultraviolet emission of the grown crystal and indicates its usefulness in the ultraviolet region.

3.6. Nonlinear optical study

Nonlinear optical activity of the compound was evaluated using SHG conversion ability by adopting the Kurtz and Perry powder method [29] using a finely powdered sample with a Q-switched Nd:YAG laser (Spiltlight compact-400, Innolas, Germany) with wavelength of 1064 nm. The pulse rate was 10 Hz and pulse diameter was 6 mm. Laser beam of energy 127 mW was incident on the sample packed between the quartz plate of 1 mm thickness, at an angle of 45°. The output light was

Table 4. The calculated fundamental parameters of LIPT and other related compounds.

Parameters	Values of LAPT [6]	Values of LHPT [5]	Values of LVPT [7]	Values of LLPT [8]	Values of LIPT (Present work)	Values of KDP [27]
Plasma energy [eV]	20.44	20.76	20.08	19.72	20.15	17.33
Penn gap [eV]	3.69	3.51	3.49	3.93	3.41	2.39
Fermi gap [eV]	16.34	16.67	16.10	15.57	16.03	12.02
Polarizability (α) by Penn analysis ($\times 10^{-23}$ cm^3)	6.83	8.36	8.61	8.91	9.83	2.14
Polarizability (α) by Clausius-Mossotti equation ($\times 10^{-23}$ cm^3)	6.87	8.62	8.65	8.93	9.09	2.18

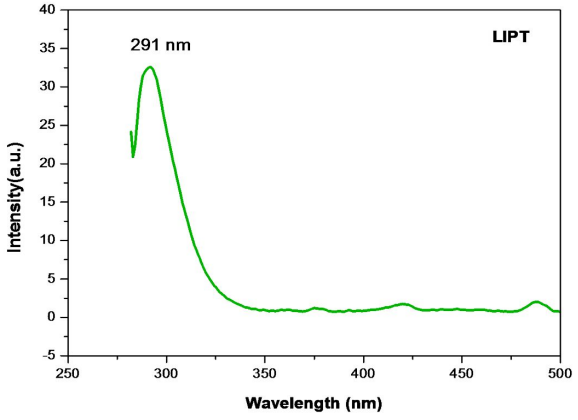

Fig. 9. Photoluminescence spectrum of LIPT.

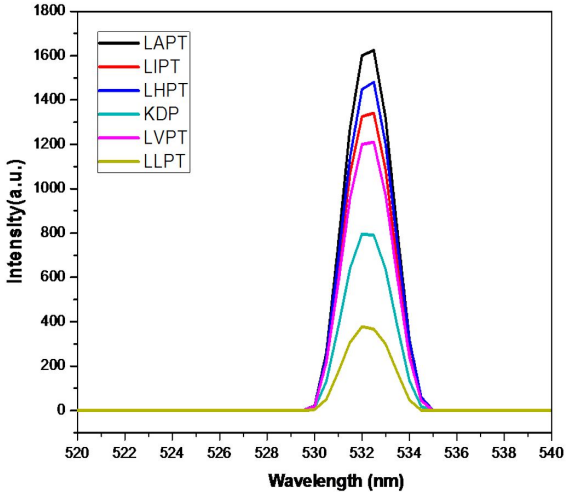

Fig. 10. SHG conversion efficiency of LIPT and related compounds.

collected at an angle 90° and passed through 532 nm interference filter to remove IR components and fed to optical fiber based UV-Vis spectrophotometer (Black Comet C-SR, Stellarnet, USA) to measure the intensity. The output intensity was measured at 532 nm and compared with the output intensity produced by KDP and other related compounds in the same setup. The experimental results are compared and shown in Fig. 10. The SHG conversion efficiencies of the title compound and its related compounds are listed in Table 5.

4. Conclusions

The newly synthesised organic NLO material L-isoleucinium p-toluenesulfonate monohydrate (LIPT) was successfully crystallized. The single crystal XRD study confirmed the non-centrosymmetric nature of the compound. The hydrogen bonding feature of the compound was analyzed. The material was thermally stable up to 110 °C. The absence of significant absorption in the entire visible region and lower cut-off wavelength indicates the suitability of the material for optical applications. The emission peak at 291 nm is an evidence of the material emission capability in the ultraviolet region. The Vicker's microhardness test showed the soft nature of the crystal. The solid state parameters calculated by dielectric studies were found to be greater than those of KDP crystal. The SHG efficiency of LIPT was found

Table 5. SHG conversion efficiency of LIPT and other related compounds

S. No.	Compound	SHG efficiency (Compared to KDP)
1.	LIPT (present study)	1.7 times
2.	L-alaninium p-toluenesulfonate (LAPT)	2.0 times
3.	L-histidinium p-toluenesulfonate (LHPT)	1.8 times
4.	L-valinium p-toluenesulfonate monohydrate (LVPT)	1.5 times
5.	L-leucinium p-toluenesulfonate monohydrate (LLPT)	0.45 times

to be 1.7 times higher than the SHG efficiency of the well-known KDP crystal. All the above findings show that the title compound LIPT may be a potential candidate for the second order nonlinear optical applications.

Acknowledgements

The authors thank SAIF, IIT MADRAS for single crystal XRD facilities. The authors also thank Dr. Gajanan G. Muley, Sant Gadge Baba Amravati University, Amravati, for SHG testing facilities.

References

[1] GUNTER P., *Nonlinear Optical Effects and Materials*, Springer-Verlag, Berlin, Germany, 2000.
[2] ZYSS J., *Molecular Nonlinear Optics: Materials, Physics, Devices*, Academic Press, New York, 1994.
[3] CRIADO A., DIANEZ M.J., GARRIDO S.P., FERNANDES I.M.L., BELSLEY M.E., DE GOMES M., *Acta Cryst. C,* 56 (2000), 888.
[4] DATTA A., PATI S.K., *J. Phys. Chem. A.*, 108 (2004), 320.
[5] SURESH M., ASATH BAHADUR S., ATHIMOOLAM S., *Optik.*, 126 (2015), 5452
[6] SURESH M., ASATH BAHADUR S., ATHIMOOLAM S., *J. Mater. Sci. Mater. El.*, 27(5) (2016), 4578.
[7] SURESH M., ASATH BAHADUR S., ATHIMOOLAM S., *J. Mol. Struct.*, 1112 (2016), 71.
[8] SURESH M., ASATH BAHADUR S., ATHIMOOLAM S., *J. Mater. Sci. Mater. El.*, 28(1) (2017), 661.
[9] YU JIN., *Acta Cryst. E*, 68 (2012), o1648
[10] ANANDHA BABU G., RAMASAMY P., *Spectrochim. Acta Part A*, 82 (2011), 521.
[11] SELVAKUMAR E., ANANDHA BABU G., RAMASAMY P., RAJNIKANT, UMA DEVI T., MEENAKSHI R., CHANDRAMOHAN A., *Spectrochim. Acta Part A*, 125 (2014), 114.
[12] PERAMAIYAN G., MOHANKUMAR R., BHAGAVANNARAYANA G., *J. Cryst. Growth*, 408 (2014), 14.
[13] REKHA P., PERAMAIYAN G., NIZAMMOHIDEEN M., MOHAN KUMAR R., KANAGADURAI R., *Spectrochimi. Acta Part A*, 139 (2015), 302.
[14] RAMASAMY G., MEENAKSHISUNDARAM S., *Optik*, 125 (2014), 4422.
[15] GEETHA P., ARULMOZHI S., MADHAVAN J., RAJ M. V. A., *Int. J. ChemTech Res.*, 6(3) (2014), 1647.
[16] SHELDRICK G. M., *Acta Cryst. C*, 71 (2015), 3.
[17] ARORA S.K., TRIVIKARAMA RAO G.S., BATRA N.M., *J. Mater. Sci*., 19(1) (1984), 297.
[18] SANGWAL K., *Mater. Chem. Phys*., 63(2) (2000), 145.
[19] HAMEED A. S. H., ROHANI S., YU W.C., TAI C.Y., LAN C.W., *J. Cryst. Growth.,* 297(1) (2006) 146.
[20] MALLIGA P., GONSAGO C.A., SAGAYARAJ P., JOSEPH ARUL PRAGASAM A., *J. Therm. Anal. Calorim.*, 110 (2) (2012), 873.
[21] BADR A. M., ELSHAIKH H.A., ASHRAF I.M., *J. Eng. Technol. Res.,* 3 (2011), 62.
[22] PAN F., WONG M.S., BOSSHARD C., GÜNTER P., *Adv. Mater.*, 8 (1996), 592.
[23] SPREITER R., BOSSHARD C.H., PAN F., GUNTER P., *Opt. Lett*., 22(8) (1997), 564.
[24] ZGONIK M., SCHLESSER R., BIAGGIO I., VOIT E., TSCHERRY J., GUNTER P., *J. Appl. Phys.*, 74(2) (1993), 1287.
[25] BALAREW C., DEHLEW R., *J. Solid State Chem*., 55 (1984), 1.
[26] BINCY I. P., GOPALAKRISHNAN R., *Opt. Mater.*, 37 (2014), 267.
[27] BELLAMY L. J., *The Infrared spectra of complex molecules*, Wiley, New York, 1975.
[28] BHAGAVANNARAYANA G., RISCOB B., SHAKIR M., *Mater. Chem. Phys.*, 126 (2011), 20.
[29] KURTZ S. K., PERRY T.T., *J. Appl. Phys*., 39 (1968), 3798.

Received 2018-03-20
Accepted 2019-03-11